Unbalance Compensation for a 5-DOF Magnetic Rotor-Bearing System

Suo-Chih Wei[a], Shyh-Leh CHEN[a]

a Department of Mechanical Engineering and Advanced Institute of Manufacturing with High-tech Innovations, National Chung Cheng University Chiayi 621, Taiwan, imeslc@ccu.edu.tw

1. Abstract

The objective of this study is to design an unbalance force rejection controller by using the decoupling control law as a levitation controller. The system under study is a 5-DOF rotor magnetic bearing system. It is equipped with two sets of heteropolar radial active magnetic bearings and one axial active magnetic bearing. In this study, an unbalance force rejection control (UFRC) structure is proposed, which is inspired by the coordinate transformation of the decoupling control. By combining the proposed UFRC controller with decoupling control, the system can be divided into two independent parts, parallel mode and conical mode. That is, the system has been decoupled. By decoupling the system, the design and analysis of the UFRC controller can be more intuitive and easier. In addition, the advantage of decoupling control is maintained. The design method and stability analysis are given in the paper. After adding UFRC controller to the control loop, the stability becomes speed dependent. Thus, the UFRC controller parameter varies for different speed range. At the end of this paper, the performance of the proposed concept is verified by numerical simulation. In summary, the proposed method works and makes the rotor turn around its center of mass so that the imbalance force is rejected. Although only the static unbalance is considered in this study, the same concept can be extended to the case where both the static unbalance and the dynamic unbalance are present.

Keywords: *Magnetic bearing, Unbalance compensation, UFRC, Decoupling control*

2. Introduction

In addition, since the magnitude of the unbalance force is proportional to the square of the speed in a magnetic bearing system, other problems such as amplifier saturation and flexible mode excitation can occur at high speeds. This is where unbalance compensation comes into play. Based on the objective, most unbalance compensation algorithms can be divided into two groups. One is unbalance vibration cancellation control (Chen, et al., 2019), which forces the rotor to rotate around its geometric axis. The other is unbalance force rejection control (UFRC) (Zheng, et al., 2016), which forces the rotor to rotate about its principal axis. In this study, a decoupling controller is used to levitate the rotor, and an UFRC controller is designed to cancel the unbalance force. The mathematical model that considers the eccentricity is introduced, and the design of the UFRC controller is investigated.

3. System description and dynamic modeling

The system under study is a 5-DOF rotor-magnetic bearing system shown in Figure 1. The rotor weight is supported by two 8-pole heteropolar active magnetic bearings at each end.

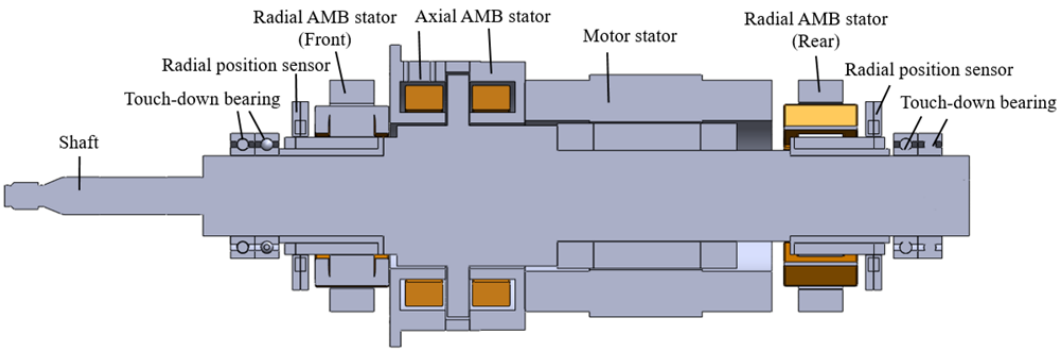

Figure 1 5-DOF rotor-magnetic bearing system

From the book by Maslen and Schweitzer (2009), if we consider only the static unbalance the rotor dynamics can be described by (1).

$$\begin{aligned} &M\ddot{q} + G\dot{q} + K_{sS}q = BK_i i_c + Us \\ &q_{se} = Cq \\ &Us = m\Omega^2 \begin{bmatrix} 0 & -e_y \sin\Omega t + e_x \cos\Omega t & 0 & e_x \sin\Omega t + e_y \cos\Omega t \end{bmatrix}^T \end{aligned} \tag{1}$$

where $q = [\beta, x, -\alpha, y]^T$, $q_{se} = [x_f, x_r, y_f, y_r]^T$. q is the body coordinate displacement of the rotor, in which x, y are displacements of the rotor and β, -α are the rotation angle of the rotor. q_{se} is the sensor coordinate displacement of the rotor, in other words, rotor displacement measured by position sensors. C is the measurement matrix. Ω is the rotation speed and e_x, e_y are eccentricities of the rotor in x, y directions respectively. M is the inertial matrix and is diagonal. To make the discussion later on easier, let us call x, y the parallel modes of the rotor and β, -α are the conical modes. Next, the decoupling PID control law we utilize to levitated the rotor is

$$i_c = -(BK_i)^{-1}\left[PC^{-1}q_{se} + IC^{-1}\int q_{se}dt + DC^{-1}\dot{q}_{se}\right] - K_{sS,comp}q_{se} \tag{2}$$

where P, I, D are diagonal and $K_{sS,comp} = -(BK_i)^{-1}K_{sS}C^{-1}$. With the control law, closed loop dynamics become (3)

$$M\ddot{q} + D\dot{q} + Pq + I\int qdt = Us \tag{3}$$

From the left side of (3), it is easy to see that the parallel and conical modes are independent. In this study, only static unbalance is considered. That is, eccentricity exists only in the radial direction of the rotor, while the axial direction of the rotor is in the absence of eccentricity. Thus, only parallel modes are affected by the unbalance force (Us), while conical modes are not. This is a nice property that we will take advantage of when designing the UFRC controller.

4. Design of UFRC controller

4.1 Block diagram of the system and UFRC controller structure

Figure 2 shows the control loop of the system, where block N represents the UFRC controller. Also, in (2), the term $K_{sS,compqse}$ is used to decouple the parallel and conical modes and must not be changed to achieve the best decoupling effect. Thus, the feedback signal is injected directly into the decoupling PID controller without passing through the UFRC controller. Figure 3 shows the structure of the UFRC controller. The error is transformed into body coordinates when it enters the UFRC controller. Before it leaves, it is transformed back to sensor coordinate. It can be seen that the concept is similar to that of the decoupling controller. Most importantly, for body coordinate errors, only parallel errors pass through the generalized notch filter (Zheng, et al., 2016), where ε, θ are parameters to be designed. This reduces the complexity of designing the notch filter parameters, since the stability of conical modes (whose pole locations are speed-dependent) is not affected by the notch filter.

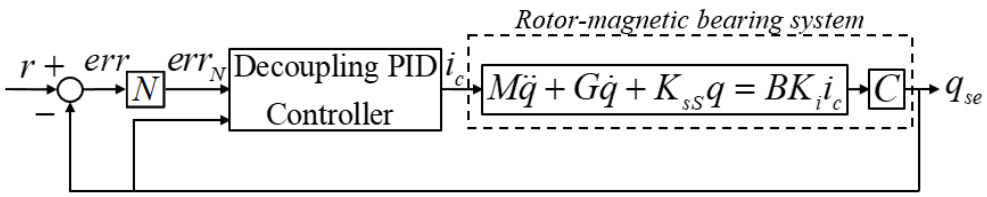

Figure 2 Block diagram of the system with controllers

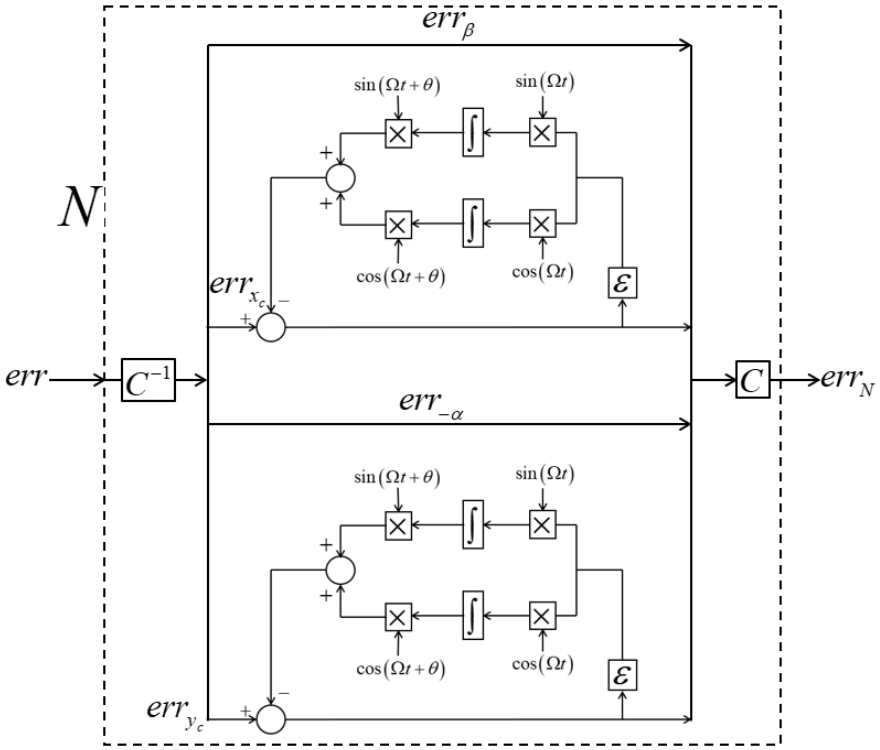

Figure 3 UFRC controller structure

4.2 Simplification of the overall system

After substituting the control law (2) and the UFRC controller structure into the block diagram shown in Figure 2, the system can be represented by the block diagram shown in Figure 4 when the rotor is not rotating. As you can see, a 4-DOF system where each DOF is coupled now becomes four 1-DOF systems where each DOF is independent. Each block in Figure 4 is as follows

$$N_{para}=\frac{s^2+\Omega^2}{s^2+\varepsilon_c s+\Omega^2-\Omega\varepsilon_s},G_{c,para}=\frac{k_{D,para}s^2+k_{P,para}s+k_{I,para}}{s},G_{c,coni}=\frac{k_{D,coni}s^2+k_{P,coni}s+k_{I,coni}}{s}$$
$$G_{P,para}=\frac{1}{ms^2},G_{P,coni}=\frac{1}{I_y s^2},\varepsilon_c=\varepsilon\cos\theta,\varepsilon_s=\varepsilon\sin\theta \quad (4)$$

N_{para} is the transfer function of the parallel mode part in UFRC controller and is of the form of generalized notch filter. $G_{c,para}$ and $G_{c,coni}$ are PID controller transfer functions correspond to parallel and conical mode respectively. Similarly, $G_{P,para}$ and $G_{P,coni}$ are plant transfer functions for parallel and conical mode respectively. $F_{unbalance}$ is the unbalance force acting on the system and can be treated as external disturbance.

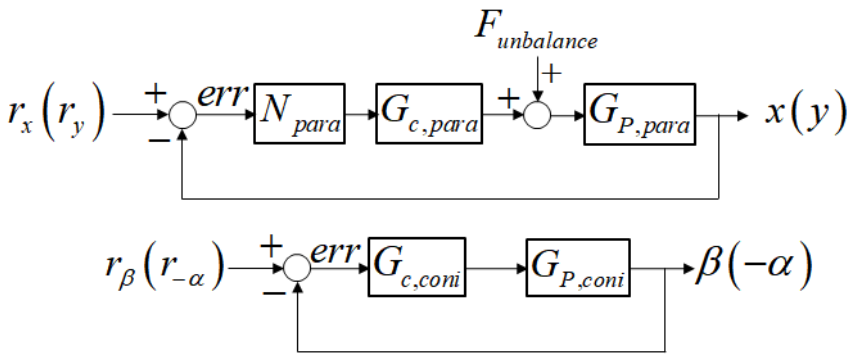

Figure 4 Block diagram of decoupled system (not rotating)

4.3 Design of UFRC controller parameter

After simplifying the system, the UFRC controller parameter design is much easier. From Figure 4, we can easily see that the conical mode block diagram has nothing to do with the notch filter design. Therefore, only the parallel mode characteristics such as stability, performance, etc. need to be investigated. Furthermore, if the dynamic unbalance is taken into account, the notch filter for each mode can be designed independently. From (4), we know that not only the UFRC controller parameter changes the system characteristics, but also the rotational speed, since N_{para} is also a function of the rotational speed Ω. Thus, the closed-loop stability of the system should be checked after introducing the designed notch filter under a certain rotational speed. In addition, since the gyroscopic effect becomes more significant and the unbalance force is stronger at high speed, the system should better preserve its characteristics at high speed after adding the notch filter. By preserving the characteristics, we can make sure that the system characteristics (sensitivity, phase margin, etc.) are similar to what we desired when designing the decoupling controller.

Let us set the operating speed as 20000 rpm, by following the above two baselines, that is, to maintain the stability and characteristics when the rotator rotates at 20000 rpm, the UFRC controller parameters are chosen as ε = 1007.1, θ = -0.1188. Figure 5 shows the dominant pole locations of the parallel mode at different speeds with this set of UFRC controller parameters. From the figure, we can see that the system loses its stability when the speed is below 3800 rpm, also the system retains its characteristics when the speed is above 6300 rpm. Note that the result in Figure 5 was obtained using the linearized model, i.e. the parallel mode block diagram in Figure 4. In the linearized model, the magnetic forces are linearized and the gyroscopic effect is not considered. To obtain a more accurate result, a nonlinear model with nonlinear magnetic force and gyroscopic effect is used for numerical simulation. The simulation result is shown in Figure 6, where UFRC is turned on when t = 1 sec. When the rotational speed is 4500 rpm and UFRC is turned on, the system reaches marginally stable, which means that the system may lose its stability when the rotational speed is below 4500 rpm. As you can see, the result is slightly different from the linear model. Thus, only when the speed is higher than 4500 rpm, the parameter set ε = 1007.1, θ = -0.1188 can be used. For speed below 4500 rpm, we need to design another set of UFRC controller parameter.

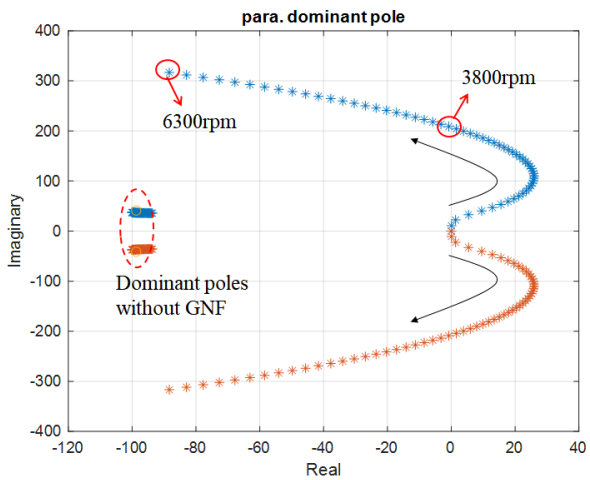

Figure 5 Parallel mode dominant pole locations under different rotation speed (UFRC on, ε=1007.1, θ=-0.1188)

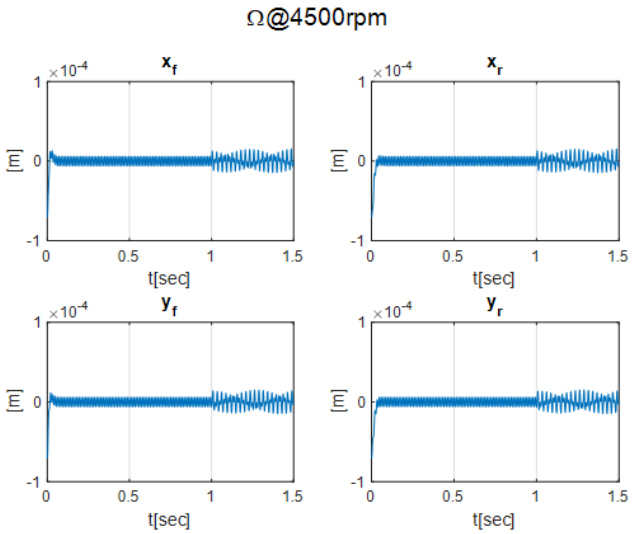

Figure 6 Rotor displacement while rotating at 4500 rpm (ε=1007.1, θ=-0.1188)

Following the same baseline, the UFRC controller parameters are chosen as ε = 200, θ = -0.0477. Figure 7 shows the dominant pole locations of the parallel mode under different rotation speed with ε = 200, θ = -0.0477. Similarly, the system loses its stability when the rotation speed falls below a certain number, which in this case is 2700 rpm. However, the dominant poles are very different from those without notch filter even at high speed, which means that the system characteristics change a lot after turning on UFRC. The simulation result with the nonlinear model is shown in Figure 8, where the UFRC is turned on when t = 1 sec. The system reaches marginally stable when the rotational speed is 2950 rpm, which is also slightly higher than the result obtained from the linear model. For the sake of safety, the first set of UFRC controller parameter is used when $\Omega > 5000$ rpm (higher than 4500 rpm) and the second set is used when $5000\text{RPM} > \Omega \geq 3100$ rpm (higher than 2950 rpm). The URFC controller parameters for different speed

ranges are shown in Table1.

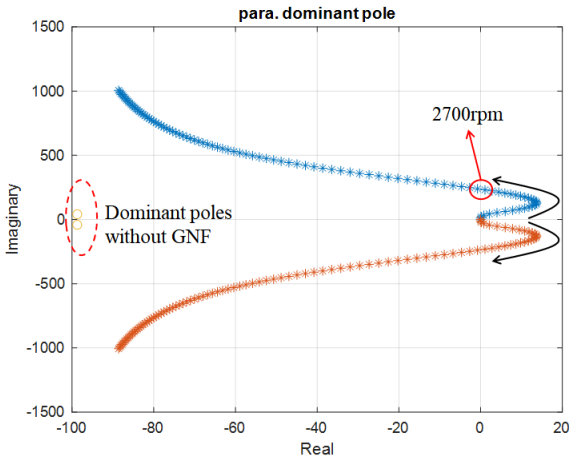

Figure7 Parallel mode dominant pole locations under different rotation speed (UFRC on, ε=200, θ=-0.0477)

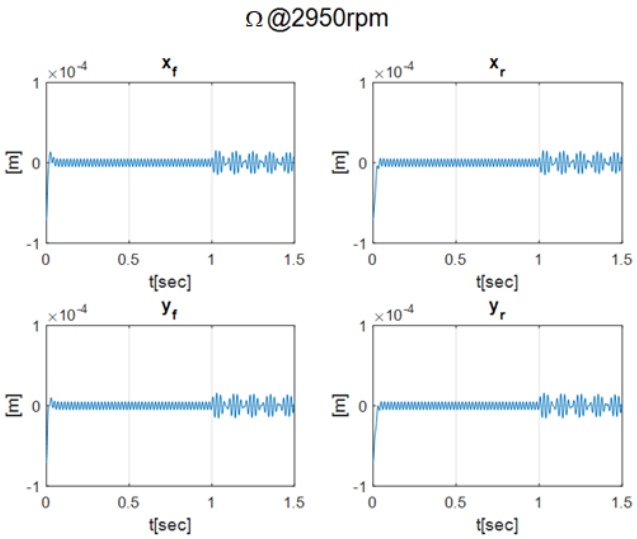

Figure 8 Rotor displacement while rotating at 4500 rpm (ε=200, θ=-0.0477)

Table 1 UFRC controller parameters for different rotation speed range

Rotation Speed [rpm]	ε	θ
5000↑	1007.1	-0.1188
3100 ~ 5000	200	-0.0477
3100↓	0	0

5. Numerical simulation

The rotation speed during simulation is shown in Figure 9. According to ISO1940-1, under the speed of 20000 rpm the maximum admissible eccentricity value is 3×10^{-3}mm. Therefore, the eccentricity of the rotor is set to e_x=3×10^{-3}mm, e_y=0. The simulation result is shown in Figure 10, where the rotor response is shown in sensor coordinates. Initially, the rotor floats from its initial position to the center without rotating. Then the rotor rotates at the speed shown in Figure 9. As can be seen in the zoomed view of Figure 10, the maximum and minimum displacement values of the one with UFRC are almost the same and are around $\sqrt{e_x^2+e_y^2}$. The same observation can be found in all other three plots, which means that the rotor is rotating around its principal axis (center of mass), causing the centroid of the rotor to oscillate.

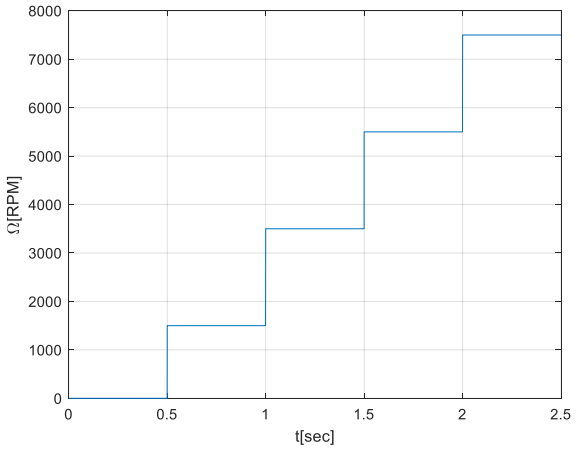

Figure 9 Rotation speed [RPM] versus time

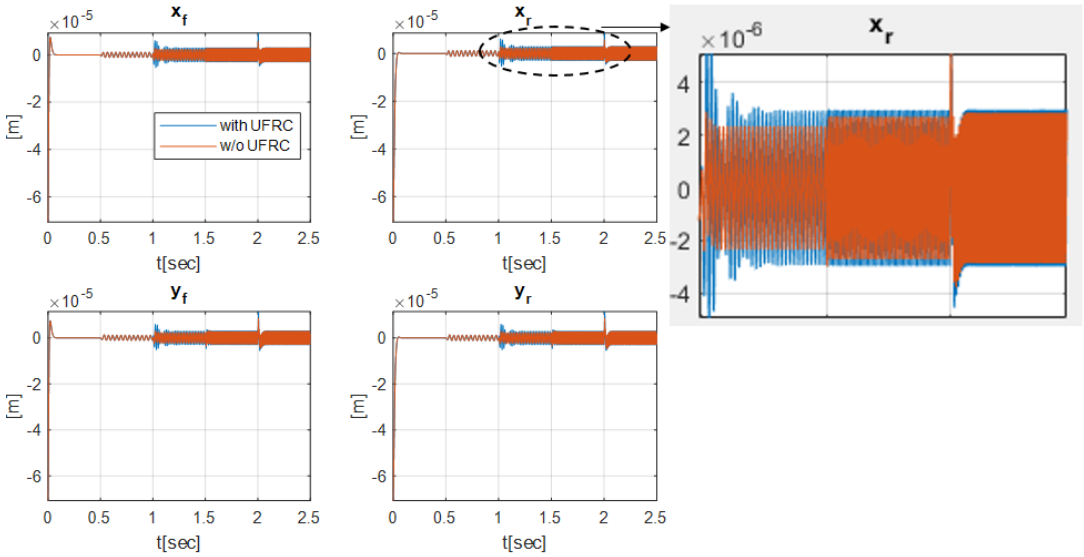

Figure 10 Sensor coordinate response versus time

6.Conclusion

In this study, a UFRC controller structure has been proposed. While using the decoupling control law as the levitation control, the UFRC controller can be easily designed. In addition, the stability of the system can also be easily verified. The UFRC controller design was shown in the paper, and its performance was verified through numerical simulation. From the simulation, the designed UFRC controller was proved to be effective.

References

[1] Chen, S.-L., S.-Y. Lin, and C.-S. Toh (2019) Adaptive unbalance compensation for a three-pole active magnetic bearing system. IEEE Transactions on Industrial Electronics 67(3): p. 2097-2106.

[2] Zheng, S., Q. Chen, and H. Ren (2016) Active balancing control of AMB-rotor systems using a phase-shift notch filter connected in parallel mode. IEEE Transactions on Industrial Electronics 63(6): p. 3777-3785.

[3] Maslen, E.H. and G. Schweitzer (2009) Magnetic bearings: theory, design, and application to rotating machinery. Berlin, Heidelberg:Springer, pp.184-185, 191-194.